Chapter 10
Noise Induced Dynamics in Adaptive Networks with Applications to Epidemiology

Leah B. Shaw and Ira B. Schwartz

Abstract Recent work in modeling the coupling between disease dynamics and dynamic social network geometry has led to the examination of how human interactions force a rewiring of connections in a population. Rewiring of the network may be considered an adaptive response to social forces due to disease spread, which in turn feeds back to the disease dynamics. Such epidemic models, called adaptive networks, have led to new dynamical instabilities along with the creation of multiple attracting states. The co-existence of several attractors is sensitive to internal and external fluctuations, which lead to enhanced stochastic oscillatory outbreaks and disease extinction. The aim of this chapter is to explore the bifurcations of adaptive network models in the presence of fluctuations and to review some of the new fluctuation phenomena induced in adaptive networks.

10.1 Introduction

In recent years, researchers have used a network approach in studying many systems, from networks of social contacts to the US power grid to the world wide web [3], and a wide variety of mathematical tools have been developed to analyze static networks [8, 26]. However, many natural systems are more complex than static network models. Both the properties of individuals (e.g., neurons, humans) and the connections between them change over time. Examples of networks where the links evolve dynamically occur in simple two state models, such as two player game theory [27, 30] and opinion dynamics [12, 32], as we will describe below.

Static network models fail to capture systems in which dynamical properties are important. A new class of models, adaptive networks, has been introduced recently to address more fully the complexity of many physical systems [18]. In an adaptive network, the network geometry changes dynamically in response to the node characteristics, and these changes in geometry then alter the subsequent dynamics of the nodes.

L.B. Shaw (✉)
Department of Applied Science, College of William and Mary, Williamsburg, VA 23187, USA
e-mail: lbshaw@wm.edu

T. Gross, H. Sayama (eds.), *Adaptive Networks,* Understanding Complex Systems,
DOI 10.1007/978-3-642-01284-6_10,

Many studies of adaptive networks have focused on steady state behavior, and rich new phenomena have been discovered in that context. However, the key aspect of an adaptive network is the interplay of node dynamics and network topology, which generally means that the nodes and links are evolving in time even if a steady state is reached. (Exceptions are cases where the network is evolved to a frozen state, as in, for example, [4, 14].) In this chapter, we consider the role of fluctuations in adaptive network models.

One property that frequently occurs in adaptive networks is self organized criticality, a topic that is discussed in more detail in the chapters of Rohlf and Bornholdt and of Caldarelli and Garlaschelli. Because each node in the network receives dynamical information that depends on the connectivity of the entire network, this can provide global information to individual nodes and cause the system to organize itself. As a result, criticality and scale free behavior are often observed. In the first adaptive network model, that of Christensen et al., adding and removing links to match a node's degree to the local average connectivity led to the network self organizing to a critical average connectivity, with a power law distribution of cluster sizes [7]. In a model by Bornholdt and Röhl motivated by neural networks, the network again organized to a critical average connectivity, balancing the addition of new links when nodes are correlated and the removal of links when nodes are uncorrelated [5]. Fan and Chen studied a growing network of chaotic maps, in which new nodes were linked to the most active previous nodes, and obtained scale free degree distributions [13]. Zhou and Kurths also obtained scale free distributions of connection weights for a network of chaotic oscillators in which the weights were evolved to increase synchrony [34]. Extensions to the latter two models are described in the chapter by Chen and Kurths.

None of the above-mentioned studies looked at fluctuations, but scale free effects on fluctuations have been observed previously. Bornholdt and Sneppen studied an evolving Boolean network, representing a genetic network, in which neutral mutations of the couplings, those that do not affect the network attractor, accumulate over time [6]. The average connectivity of the network was monitored, and long periods of stasis in connectivity were interrupted by bursts of connectivity change. The stasis times followed a scale free distribution. In a model for an evolving network of chemical species, in which species that do not multiply as quickly are replaced by new random species, Jain and Krishna observed similar fluctuations in the number of populated species [25]. In the long time limit, all species are usually populated, but this value is punctuated by drop-out times due to the disruption of autocatalytic sets. Jain and Krishna did not do a statistical analysis of this effect, but their time series are reminiscent of punctuated equilibria.

In evolutionary game theory models with perturbations, scale free distributions have been observed for the sizes of avalanches (number of nodes involved) as the system moves between stationary states (e.g., [11, 28]). A model by Holme and Ghoshal for nodes that rewire the network to maximize their social influence and change their rewiring strategies adaptively also displayed avalanches in strategy changes, but statistics were not collected on the scaling of the avalanche size [20].

The degrees and cluster sizes in this model also fluctuated significantly. This model is discussed in detail in the chapter by Holme and Ghoshal.

Another effect that is observed in adaptive network models for opinion formation in social networks is the existence of metastable states. Ehrhardt and Marsili studied a model in which new links were generated preferentially between nodes with a similar "opinion" or property, and the opinions were influenced by neighbor nodes [12]. In the limit where the nodes were at zero temperature (but links were added and removed stochastically), the system eventually approached one large connected component with uniform opinion, but it spent time in metastable states with multiple components, each with different opinion. The lifetimes of the metastable states could be understood analytically through an exact solution and stability analysis of the zero temperature case.

Holme and Newman developed a model for opinion dynamics in which a parameter governed the relative frequencies of rewiring to new neighbors with identical opinions versus convincing one's neighbors to share one's opinion [21]. The system evolved to a frozen state containing one or more communities, where the number of communities depended on whether the parameter favored convincing or rewiring. The parameter controlled a continuous phase transition, and at the critical value the system exhibited a power law distribution in community sizes and large fluctuations in the time required to converge to the final state. The nature of the phase transition was further explained analytically by Vazquez et al. for a simpler model with only two opinion states [31]. A variety of models of opinion formation are described in detail in the chapter by Do and Gross.

Other adaptive network models have considered synchrony of a network of coupled oscillators while adjusting the network connections adaptively [15, 16, 23, 24, 34]. Gong and Leeuwen studied networks of coupled chaotic maps and added connections between correlated oscillators [16]. They found that the system formed a small world network with intermittent switching in the number of coherent clusters. Ito and Kaneko studied weighted networks of coupled maps and also strengthened the coupling between correlated oscillators [23, 24]. Here they considered in detail the role of the feedback mechanism between node and network dynamics. The model is also discussed in the chapter by Ito and Kaneko. They computed average weight matrices to determine whether there were stable structures in the network and found several phases, including a phase that was desynchronized but had a temporarily stable network structure, and a desynchronized phase with a disordered, rapidly changing network structure [24]. In the disordered network structure, the degree of individual nodes changed almost randomly. However, in the networks with temporarily stable structure, the nodes separated into two groups, controllers with high outdegree and others with low outdegree. The group in which a given node resided remained relatively stable over time. The node dynamics in the desynchronized phase was characterized by hopping between two groups whose dynamics were a half cycle out of phase from each other. In a feedback loop between the network geometry and node dynamics, nodes that hopped more slowly between groups tended to accumulate more connections, which led to further slowing of the

hopping rate. This feedback loop was responsible for the splitting of the nodes into high outdegree and low outdegree groups.

Effects such as self organized criticality, metastable states, and fluctuations in synchrony have been observed in adaptive networks. Thus far, these effects have mainly been quantified through simple network metrics such as time series of the average connectivity or clustering coefficient, or the average node properties may be tracked over time as will be discussed later in this chapter. When the network forms distinct clusters, tracking the number of clusters is also an option. However, higher order network structures are often difficult to track in a time-varying network, and it is not yet clear what are the key network properties to measure for an adaptive network. Also, in many cases the effects that have been observed have not yet been explained analytically. Further study of the fluctuations in adaptive networks is needed.

In this chapter, we focus on fluctuations in a model for an epidemic spreading on an adaptive network. Epidemics have been briefly mentioned in the previous chapter. Some of the results in the present chapter have been published elsewhere [29]. The layout of the paper is as follows: We describe the model and summarize key aspects of its bifurcation structure in Sects. 10.2 and 10.3. Many properties can be predicted from a much lower dimensional mean field model. In Sect. 10.4, we focus particularly on fluctuations in the number of infection cases in the system, which is a physically important quantity. We present some additional results for phase relationships between node and link variables and for scaling of the epidemic lifetime in Sects. 10.5 and 10.6. The dynamic network structure is more difficult to capture, but in Sect. 10.7 we discuss fluctuations in the degree of individual nodes in the system.

10.2 Model

Gross et al. have introduced a susceptible-infected-susceptible (SIS) model on an adaptive network [19], and Zanette and Gusmán have also studied an SIS model on an adaptive network [33]. We have extended this work to a susceptible-infected-recovered-susceptible (SIRS) model [29]. Although we have not chosen parameters corresponding to a particular real disease, tuning the average time a node spends in the recovered class allows us to adjust the average number of infections at the endemic steady state. Although some diseases in the past, such as plague, have eliminated as much as 50% of a worldwide population, many infectious viral diseases, such as measles, mumps, and rubella, infect only 10% or less of a population at a given time [1], depending on epidemiological and social factors. Noise effects are expected to be especially prominent when the infection occurs at low levels. However, in this particular study, we restrict our attention to cases where the minimum endemic steady states are on the order of 10–40% of the population.

Our model is constructed as an extension to that of Gross et al. [19] but includes the addition of a recovered class. The rate for a susceptible node to become infected is $pN_{I,\mathrm{nbr}}$, where $N_{I,\mathrm{nbr}}$ is the number of infected neighbors the node has. The

recovery rate for an infected node is r. We fix $r = 0.002$ throughout this chapter. A recovered node becomes susceptible again with rate q, the resusceptibility rate.

Since the mean time spent in the recovered state is $1/q$, there is a natural limiting case for the SIRS model. Using the recovery rate, r, as a natural time scale, as the ratio q/r becomes sufficiently large, nodes spend less time in the recovered state. In the limit $q/r \to \infty$, the model thus approaches the SIS model. The study of the stochastic dynamics of the SIRS model may then be examined with respect to changes in q.

Rewiring of the network occurs as the epidemic spreads. If a link connects an infected node to a non-infected node, the link is rewired with rate w. The connection to the infected node is broken, and the original non-infected node is now connected to another non-infected node which is randomly selected out of all candidates in the network (excluding self links and multiple links between nodes). This rewiring rule is that of Gross et al. [19] (we treat the recovered nodes in the same manner as susceptibles for rewiring purposes), in contrast to the rewiring scheme of Zanette and Gusmán [33], which allows susceptible nodes to connect to infectives.

We performed Monte Carlo simulations of this model for a system with N nodes and K links, where K/N was fixed at 10. Details of the simulation procedure can be found in [29]. Random sequential updating was used, and each node and eligible link had an opportunity to transition on average once per Monte Carlo step (MCS).

As in [19], we developed a corresponding mean field model using a moment closure approximation to track the dynamics of nodes and links. P_A denotes the probability for a node to be in state A, and P_{AB} denotes the probability for a link to connect a node in state A to a node in state B. For higher order correlations, we assume $P_{ABC} \approx P_{AB}P_{BC}/P_B$. The time evolution of the node states is described by:

$$\dot{P}_S = q\,P_R - p\tfrac{K}{N}P_{SI} \tag{10.1}$$

$$\dot{P}_I = p\tfrac{K}{N}P_{SI} - r\,P_I \tag{10.2}$$

$$\dot{P}_R = r\,P_I - q\,P_R \tag{10.3}$$

The time evolution of the links is described by:

$$\dot{P}_{SS} = q\,P_{SR} + w\tfrac{P_S}{P_S+P_R}P_{SI} - 2p\tfrac{K}{N}\tfrac{P_{SS}P_{SI}}{P_S} \tag{10.4}$$

$$\begin{aligned}\dot{P}_{SI} = {} & 2p\tfrac{K}{N}\tfrac{P_{SS}P_{SI}}{P_S} + q\,P_{IR} - r\,P_{SI} - w\,P_{SI} \\ & -p\left(P_{SI} + \tfrac{K}{N}\tfrac{P_{SI}^2}{P_S}\right)\end{aligned} \tag{10.5}$$

$$\dot{P}_{II} = p\left(P_{SI} + \tfrac{K}{N}\tfrac{P_{SI}^2}{P_S}\right) - 2r\,P_{II} \tag{10.6}$$

$$\begin{aligned}\dot{P}_{SR} = {} & r\,P_{SI} + w\tfrac{P_R}{P_S+P_R}P_{SI} + 2q\,P_{RR} - q\,P_{SR} \\ & -p\tfrac{K}{N}\tfrac{P_{SI}P_{SR}}{P_S} + w\tfrac{P_S}{P_S+P_R}P_{IR}\end{aligned} \tag{10.7}$$

$$\dot{P}_{IR} = 2r P_{II} + p\frac{K}{N}\frac{P_{SI}P_{SR}}{P_S} - q P_{IR} - r P_{IR} - w P_{IR} \tag{10.8}$$

$$\dot{P}_{RR} = r P_{IR} - 2q P_{RR} + w\frac{P_R}{P_S+P_R} P_{IR} \tag{10.9}$$

We integrated the mean field equations numerically and tracked their steady states using a continuation package [9]. We have also considered a stochastic mean field system with internal fluctuations, modeled by multiplicative noise, or with external fluctuations, modeled by additive noise. The stochastic mean field system was studied using a fourth order Runge-Kutta solver.

10.3 Bifurcation Structure

In [29], we considered the bifurcation structure of the mean field for q small and mapped the regions of stability for infectives as a functions of the parameters w and p. We discovered and reported that there were regions of q in which different bifurcation scenarios existed, as well as regions of bistability. In the first case, the value of $q = 0.0064$, the disease free equilibrium became unstable as the infection rate p was increased, and through a transcritical bifurcation was connected to the unstable branch of endemic states. A stable branch of endemic states was then connected to the unstable branch via a saddle-node bifurcation. However, in the second case, that of $q = 0.0016$, there is no saddle-node bifurcation. Instead there exists a saddle-saddle connection. In this case, the unstable endemic state emanating from the disease free state has a one-dimensional unstable manifold. This branch is connected via a turning point to an unstable endemic branch having a two-dimensional unstable manifold, which in turn becomes stable through a Hopf bifurcation.

The bifurcation diagram for this case is reproduced here for clarity of discussion in Fig. 10.1. For the saddle-saddle case, the lower (upper) branch has a one (two) dimensional unstable manifold. The upper branch then undergoes a reverse Hopf bifurcation. The connecting branch of periodic orbits (not shown) is unstable and sub-critical. These orbits have very long periods and large swings in amplitudes of infectives.

Recalling that q controls the resusceptibility rate and w the rewiring rate, we examine the structure of the bifurcation onset of attracting endemic states while holding the other parameters fixed. The onset of Hopf bifurcation points in two parameters was computed, and is shown in Fig. 10.2, for both the mean field model and the full system. Bifurcation points in the full system were estimated as the largest w value for which a single run started near the probable endemic steady state remained near that state for 10^5 MCS without dying out. The region below the curve contains stable endemic branches, while the region above contains unstable endemic states and/or stable disease free equilibria. The same trends are observed in both the mean field and the full system. Notice that for q greater than approximately 0.3, the value of w for the Hopf bifurcation does not change much. In addition, the infective fraction is also approximately independent of q for q sufficiently large,

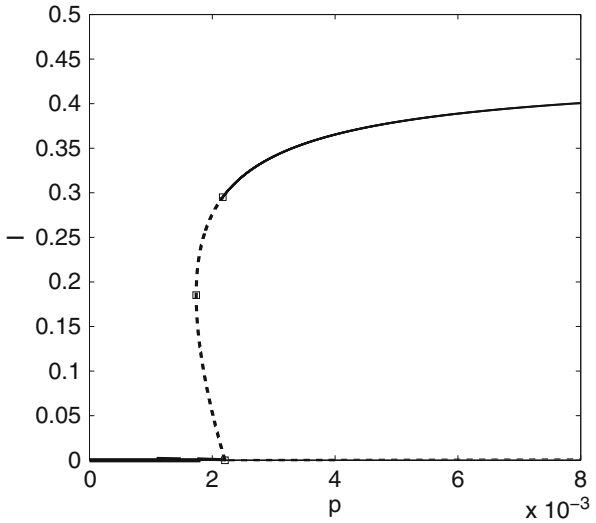

Fig. 10.1 A bifurcation diagram of the infective fraction as a function of p, with $w = 0.04$, $r = 0.002$, $q = 0.0016$. The *squares* denote the saddle–saddle point and transcritical point. *Dashed lines* are unstable branches. As p is decreased, the endemic state loses stability in a Hopf bifurcation

signifying that the model is approaching the SIS model. One would typically expect that as the resusceptibility rate q increases, the number of nodes that are in the recovered state and thus protected from infection will decrease, and the infection will spread more easily. Therefore, a faster rewiring rate (larger w) will be needed to suppress the infection. Indeed, this is the trend observed in Fig. 10.2 for small

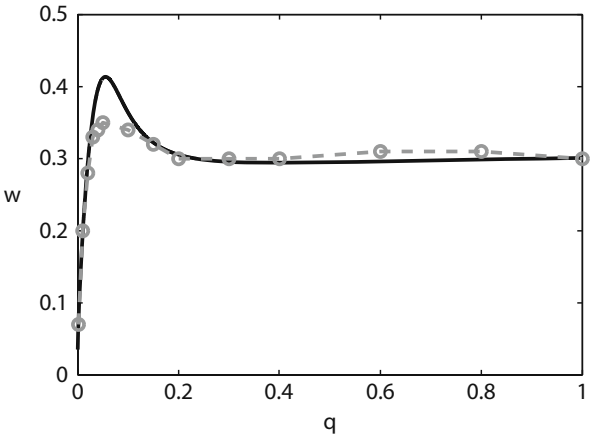

Fig. 10.2 A two parameter diagram of the Hopf bifurcation points as a function of q and w. *Solid curve*: mean field model; *points* and *dashed curve*: full system. Parameters used are $r = 0.002$, $p = 0.004$

and large q. However, the w value for the bifurcation decreases with increasing q between about 0.1 and 0.2. This nonmonotonic shift in the bifurcation point in Fig. 10.2 is a nonlinear effect which has not yet been explained.

In later sections we will explore the fluctuations of the SIRS model for values of q between the values 0 and 1. Effects on the fluctuations of the nonmonotonic bifurcation curve in Fig. 10.2 have not been observed.

We remark that a direct comparison in [29] of the infective fraction between the mean field model and Monte Carlo simulation of the full system showed excellent agreement along the attracting branches. The discrepancies occurred near the bifurcation point where the endemic state loses stability, partly because the actual location of the instability in the full stochastic system was difficult to detect accurately in Monte Carlo simulations and partly due to inaccuracies in the mean field approximation. However, the scaling results near the bifurcation, which we present in the next section, are generally consistent between the mean field model and the full system.

10.4 Effect of Recovered Class on Fluctuations

We have observed that the amplitude of fluctuations in the number of infectives is generally larger in the SIRS model than the SIS model. In the SIS system, links between two infectives are not broken because rewiring operates only on SI links. Thus when an infective becomes susceptible again, the newly formed susceptible may be connected to other infectives that it retained as neighbors while previously infected and can immediately become reinfected. This situation tends to suppress fluctuations, because small decreases in the total number of infectives correspond exactly to increases in the number of susceptibles, and rapid reinfection of the susceptibles can occur, preventing the number of infectives from dropping significantly. In the SIRS model, on the other hand, the recovered compartment introduces an effective time delay from recovery to possible reinfection and allows infective levels to fluctuate more.

Figure 10.3 compares the scaling of fluctuations near the bifurcation point for two different values of the resusceptibility rate q. In the top panels $q = 0.0016$, the rate used in [29]. In the bottom panels $q = 1$, effectively approximating the SIS case, since individuals spend very little time in the recovered class and much less than 1% of the population is in the recovered class at a given time. Fluctuations in the infectives (measured as the standard deviation divided by mean for long Monte Carlo simulations) are plotted as a function of p, the infection rate, as p is swept towards the bifurcation point. Results were computed from 5×10^5 MCS time series sampled every 10 MCS. The magnitude of the fluctuations is greater for the SIRS case (Fig. 10.3a) than for the SIS case (Fig. 10.3c). Notice that the increase in fluctuations is almost an order of magnitude.

The fluctuations exhibit power law scaling, shown in the log–log plots in Fig. 10.3b, d. On the horizontal axis, we plot $\ln(p - p_c)$, where p_c is the critical point at which the endemic state loses stability. The bifurcation points are not known

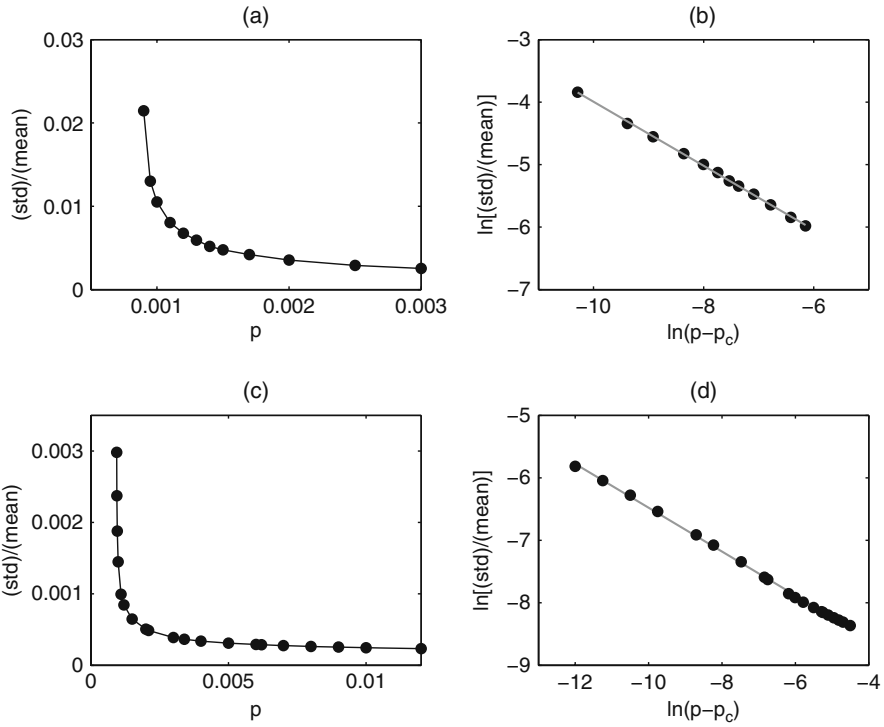

Fig. 10.3 Fluctuations in infectives (standard deviation divided by mean) vs. infection rate p near the bifurcation point, from Monte Carlo simulations: (**a**) $q = 0.0016$ (SIRS case), (**c**) $q = 1$ (approximately SIS case). *Curves* are to guide the eye. Log–log plots (data points with best fit lines) show power law scaling for both $q = 0.0016$ (**b**) and $q = 1$ (**d**). Other parameters: $w = 0.04$, $r = 0.002$. Parts (**a**) and (**b**) are reprinted from [29]

exactly, so we approximate p_c by the value that produces the most linear plot in each case. For the data of Fig. 10.3, the scaling exponents are similar (-0.59 versus -0.51 for $q = 0.0016$ and 1 respectively), so it is not clear that the resusceptibility rate has a significant effect on how the fluctuations scale with p.

The power law scaling of the fluctuations can be understood by considering the scaling near a generic bifurcation point. From our mean field analysis, we expect the bifurcation point where the endemic steady state loses stability to be either a saddle-node bifurcation point or a Hopf point. A generic saddle-node bifurcation exhibits power law scaling of fluctuations near the bifurcation point, as we show in Fig. 10.4 and explain in the discussion below. A Hopf bifurcation can also appear locally to have power law scaling of fluctuations, although the scaling may be over a smaller range of parameters. For a given standard deviation, the probability density function near a Hopf bifurcation is given by [2]:

$$p_{hb}(\beta, r, \sigma, R) = Nr^{\frac{\beta}{\sigma^2}} e^{-\frac{Rr^2}{\sigma^2}} \sigma^{-2} \left[\Gamma\left(1 + 1/2\,\frac{\beta}{\sigma^2}\right) \right]^{-1} \tag{10.10}$$

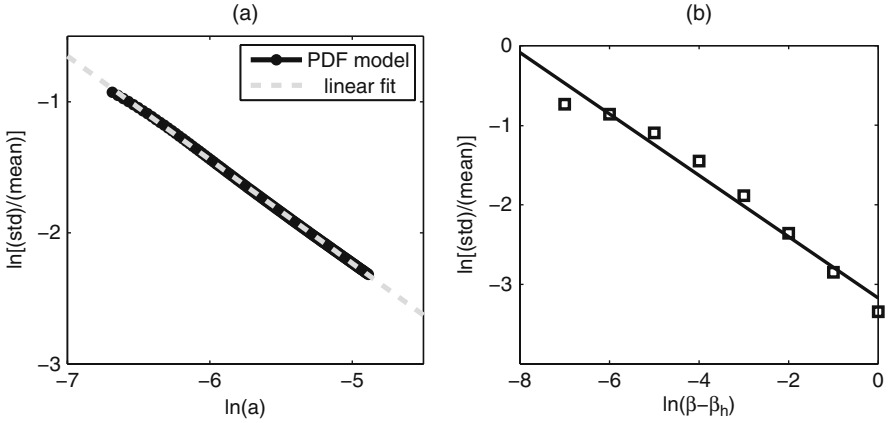

Fig. 10.4 (**a**) Fluctuation size of a generic saddle-node bifurcation as a function of bifurcation parameter a near the bifurcation point using the probability density function in Eq. (10.12). Noise amplitude is $\sigma = 0.005$. (**b**) Fluctuation size of a generic Hopf bifurcation as a function of bifurcation parameter β near the bifurcation point using the PDF in Eq. (10.10) (*squares*). The *line* is a best linear fit. Noise amplitude is $\sigma = 0.05$.

where the state space variable is a radial coordinate r, β is the distance from the Hopf bifurcation point, parameter $R = 0.5$ is fixed, Γ is the gamma function, and N is a normalization constant. An example of the fluctuations using Eq. (10.10), where we have computed the first and second order moments to find the ratio of the standard deviation to the mean, is shown in Fig. 10.4b. The data for the fluctuation size deviates from a power law scaling, as exhibited in the figure. However, there is a monotonic relationship in the fluctuations as measured by σ/μ as a function of the distance to the Hopf bifurcation. Therefore, we expect the fluctuation characteristics of the SIS and SIRS models to hold near bifurcation points regardless of whether the statistics are measured with respect to a Hopf or saddle-node bifurcation.

Since the power law scaling is observed near either a saddle-node or Hopf bifurcation point, it may be understood by considering the local dynamics. For example, near the saddle-node, a center manifold reduction would reduce the study of the vector field to a system with a one-dimensional unstable manifold. Therefore, the power law scaling of the fluctuations can be motivated by considering the following simple stochastic differential equation

$$dx_t = (a - x_t^2)dt + \sigma * dW_t \tag{10.11}$$

for a one dimensional saddle-node bifurcation, where a is the bifurcation parameter, dW/dt is a white noise term, and dW is a Brownian increment. In general, noise can cause a shift in the location of the saddle-node bifurcation, so we assume that the noise is sufficiently small that the location is fixed.

By assuming we are always near the attracting branch of the saddle-node or Hopf bifurcation, we are in a near equilibrium setting driven by noise. Such an

assumption allows us to examine the stationary probability density function (PDF) of the stochastic dynamics by employing the Fokker-Planck equation near steady state. For the stochastic differential equation, Eq. (10.11), the PDF is well known [22] and is given by

$$p(a, x, \sigma) = Ne^{2(ax - x^3/3)/\sigma^2}. \tag{10.12}$$

Here N is a normalization constant. From Eq. (10.12), we compute the first and second order moments to find the ratio of the standard deviation to the mean. We examine the fluctuations in the neighborhood of $a = 0$, which is the location of the saddle-node point. The results display power law scaling, as depicted in Fig. 10.4a.

To further examine the differences in fluctuations between the SIS and SIRS adaptive network models, we perform the following experiment. As discussed above, we can examine the fluctuation sizes as a function of resusceptibility rate q to see how the fluctuation sizes compare between the two model classes. The other variable which controls the recovered, as well as the infected, populations is the rewiring rate, w. It has a significant effect on the fluctuations, since the degree of infectives is dramatically reduced by the rewiring. We examine the interplay between q and w and their effect on fluctuation sizes. Here we turn to a stochastic version of the mean field model. We have shown previously that the scaling behavior of the mean field model is typically similar to that of the full network system [29].

We use additive noise to model fluctuations near the endemic equilibrium state. Details may be found in [29]. The stochastic mean field model has the following form:

$$\mathbf{X}' = \mathbf{F}(\mathbf{X}) + \varepsilon\eta(\mathbf{t}), \tag{10.13}$$

where $\mathbf{F}(\mathbf{X})$ is the mean field system in Eqs. (10.1)–(10.9), $\eta(\mathbf{t})$ is a noise term with $\langle\eta(\mathbf{t})\eta(\mathbf{t}')\rangle = \delta(\mathbf{t} - \mathbf{t}')$, and ε is the noise amplitude. Fluctuations are computed by averaging the standard deviation over mean results for time series starting from 10 random initial conditions near steady state. The runs were computed for 5×10^7 steps using a step length of 0.001, and transients were removed after 10^6 steps.

A typical example of the fluctuations as w is varied is shown in Fig. 10.5b. Similar linear log–log behavior is observed in other stochastic simulations for other values of q. In Fig. 10.5b, w_h denotes the location of the Hopf bifurcation branch. The Hopf bifurcation occurs for all values of q considered here. A typical bifurcation plot is shown in Fig. 10.5a for $q = 0.1$. Attracting states are solid curves, while unstable states are dashed and dotted curves. The Hopf bifurcation point is on the upper branch separating the stable and unstable steady states.

Because of the power law scaling of the fluctuations, as in Fig. 10.5b, we expect a functional relationship of the form

$$\sigma(q)/\mu(q) \propto [w_h(q) - w]^{m(q)} \tag{10.14}$$

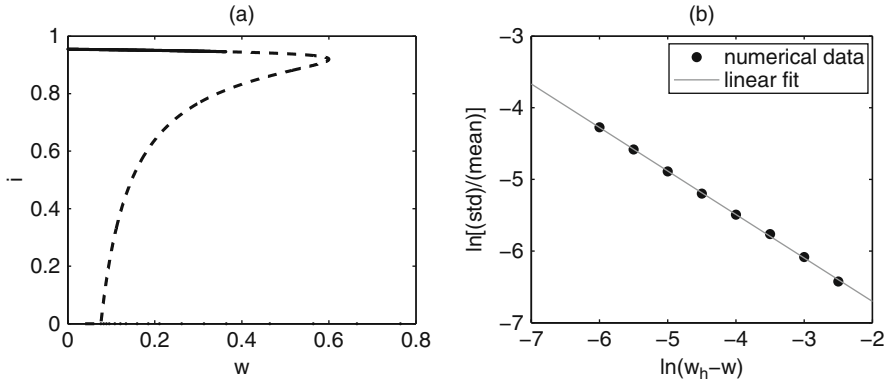

Fig. 10.5 (**a**) A bifurcation plot of the mean field model without noise. Plotted is the fraction infected as a function of w. Parameters are $r = 0.002, p = 0.004, q = 0.1$. (**b**) Plot of the fluctuation sizes as a function of rewiring rate, w. The fixed parameters used are $r = 0.002,\ p = 0.004,\ K/N = 10,\ q = 0.01, \varepsilon = 0.0001$

where $m(q)$ is the average slope of the log–log plots. We can now examine how the average rate of change of fluctuations varies as a function of q. The results are shown in Fig. 10.6. At smaller q values, the fluctuations increase more quickly with w than they do in the large q limit. Therefore, the fluctuations are more sensitive with respect to w in the SIRS model than in the SIS model.

We attempted to confirm this mean field result for the slopes using the full model, but in the case of the full model, the exact locations of bifurcation points are unknown. It is difficult to estimate where the endemic state loses stability from time series because one cannot always distinguish a metastable state from a stable state in the presence of fluctuations. We can approximate the bifurcation point by the value that gives the most linear plot (largest R value) for fluctuations vs. the

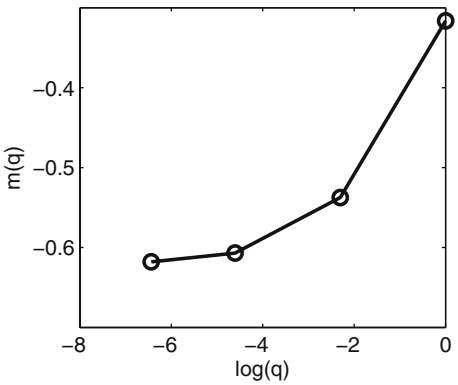

Fig. 10.6 A plot of the slope $m(q)$ as a function of q. See text for details. Parameters used are $r = 0.002, p = 0.004, \varepsilon = 0.0001$

bifurcation parameter as in Fig. 10.3, but this approach is unreliable if the scaling deviates from a power law, as occurs in Fig. 10.4b for a generic Hopf bifurcation. The best fit slope depends sensitively on the estimate for the bifurcation point, so we were not able to obtain robust results for the full system.

10.5 Delayed Outbreaks

We have also considered phase relationships between the fluctuating node and link variables. At each time point in our simulations, we tracked the number of infected nodes as well as the number of non-infected neighbors of infected nodes (which corresponds to the number of SI and IR links). The rewiring causes the fluctuations in the number of infectives to lag behind fluctuations in the number of infective neighbors, as shown in Fig. 10.7a. This effect was observed both in the mean field model (data not shown, see [29]) and in Monte Carlo simulations of the full system.

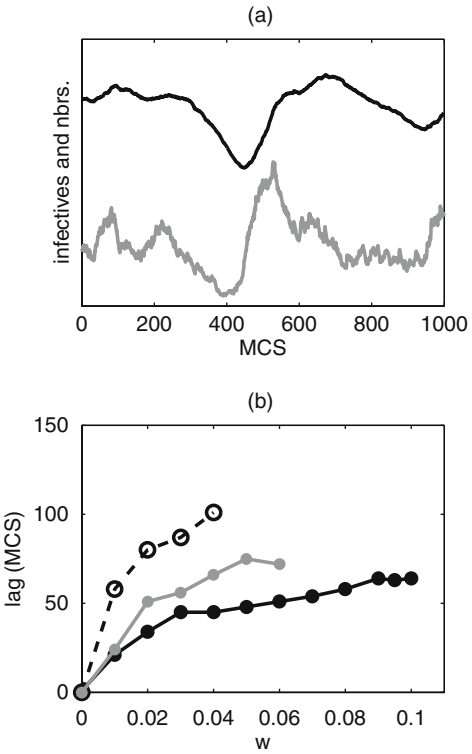

Fig. 10.7 Delayed outbreaks due to rewiring. (**a**) Monte Carlo time series. *Black*: infectives; *gray*: neighbors of infectives. *Curves* are scaled in arbitrary units for comparison of peak times. $p = 0.0065, w = 0.09, q = 0.0016, r = 0.002$. Reprinted from [29]. (**b**) Time in MCS by which infectives lag behind infective neighbors vs. rewiring rate. *Solid black*: $q = 0.0016$; *gray*: $q = 0.001$; *dashed black*: $q = 0.0005$. Other parameters: $p = 0.0065, r = 0.002$

We studied the dependence of this phase lag on both the rewiring rate w and the resusceptibility rate q when the system was fluctuating around the endemic steady state. Monte Carlo simulations were sampled every 1 MCS for 3×10^4 MCS after discarding transients. We computed cross correlations between the infectives and the infective neighbors for varying phase shifts between the two time series and identified the lag maximizing the cross correlation. Figure 10.7b shows results for three different q values. (Note: Curves for smaller q terminate at lower w values because the endemic steady state becomes unstable, as in Fig. 10.2.) In each case, the lag increases with increasing rewiring rate. This effect does not have a simple explanation, but since it is also observed in mean field simulations, it depends on node and link dynamics primarily, rather than higher order geometries.

Further, the lag time increases as the resusceptibility rate q decreases. This occurs because the recovered class introduces an effective delay in the system. When a node becomes at risk because its neighbor is infected, it cannot itself become infected until it is susceptible. As q is lowered, the fraction of infective neighbors that are recovered and have to wait to become susceptible again increases, and the average wait time also increases, so it is expected that the infective fluctuations will lag further behind.

It should be noted that when $q = 1$ and the system approximates the SIS model, the number of infectives and non-infected neighbors of infectives (i.e., SI links) are poorly correlated for any shift between time series. Therefore, the lags discussed here are not observed in the SIS model.

10.6 Lifetime of the Endemic Steady State

Another effect we consider, which depends on fluctuations in the system, is the lifetime of the endemic steady state. Because the system is stochastic and the disease free state is absorbing, the disease will die out in the infinite time limit for any set of parameters. For a generic saddle-node bifurcation in one dimension, the scaling of the lifetime is expected to obey

$$\ln T \propto (p - p_0)^{3/2}, \tag{10.15}$$

where T is the mean dwell time or lifetime of the steady state, p is the bifurcation parameter, and p_0 is the location of the bifurcation point [10, 17]. Using the computational methods in [29], we show preliminary results for the dependence of the lifetime on the infection rate p in Fig. 10.8. The bifurcation point p_0 was estimated by the value that gave the most linear plot for $\ln T$ vs. $(p-p_0)^{3/2}$. The scaling results appear consistent with expectations, but further study is needed. In contrast to the mean field model, because the exact location of bifurcation points is not known for the full system, details such as slopes and scaling exponents can be very much dependent on estimates for the bifurcation point.

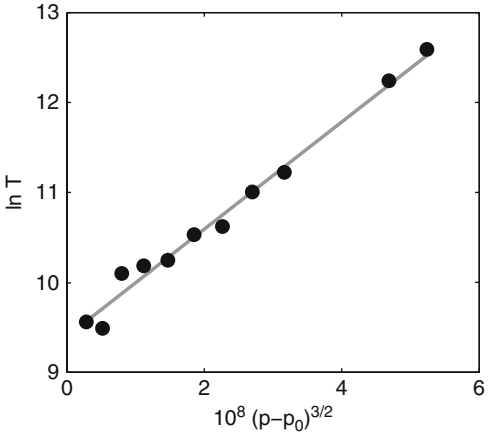

Fig. 10.8 Dependence of endemic state average lifetimes T on infection rate p. *Points*: Monte Carlo simulations; *line*: best fit line. $q = 0.0016$, $r = 0.002$, $w = 0.04$, $N = 4 \times 10^4$, $K = 4 \times 10^5$. (Reprinted from [29].)

10.7 Network Geometry

Defining appropriate statistics to capture a fluctuating network geometry is difficult. Here, the network does not display community structure nor is governed by an underlying spatial structure. Links are rewired to any acceptable target nodes, regardless of distance away. Because the mean field theory for nodes and links captures the dynamics of the system fairly well, higher order correlations involving three or more nodes do not have a large impact on the dynamics. The network may be fairly unstructured at the higher levels.

To demonstrate the role of fluctuations in the network geometry on the scale of individual nodes and links, we show in Fig. 10.9 the time-varying degree of a single arbitrarily chosen node. When the node becomes infected, its non-infected neighbors quickly rewire away from it (dashed gray curves). Because infected neighbors do not rewire away, the degree may not drop all the way to zero before pausing. If the infected node remains infected for sufficiently long, its neighbors will recover and then rewire away, further decreasing the degree. Once the node recovers, other S and R nodes in the system may rewire to it, and its degree begins to climb (black curves). When the node becomes susceptible, the degree continues increasing (solid light gray curves) until the node again becomes infected, and the cycle repeats.

It is not yet known how to predict the degree distributions from first principles [29], but if one assumes that the degree distributions are already known for each node class, the fluctuations in the degree of a single node can be easily understood. Figure 10.10 shows the statistics of the local maxima and minima of the degree time series for a single node. Results are computed for a 4×10^6 MCS time series, which contains approximately 2,000 SIRS transition cycles (and thus approximately

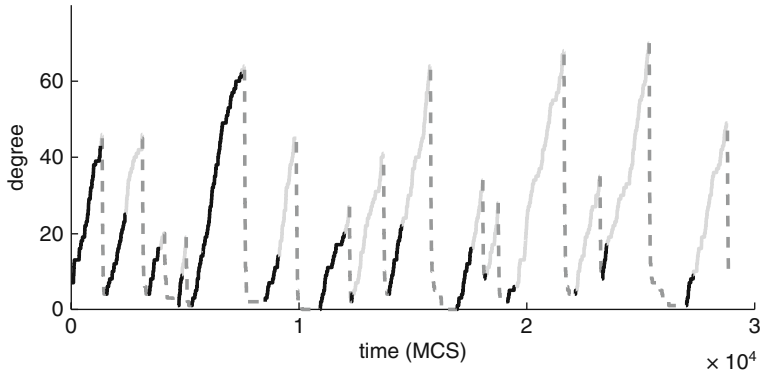

Fig. 10.9 Degree of a single node versus time. *Curves* indicate the node's disease status: *black*: recovered; *light gray*: susceptible; *dashed medium gray*: infected. Parameters: $p = 0.002$, $q = 0.0016$, $r = 0.002$, $w = 0.04$

2,000 maxima and minima). Frequency distributions for the maxima (Fig. 10.10a) and minima (Fig. 10.10b) are shown.

The minima can be most easily understood. Minima occur when an infective recovers. Recovery is governed by the rate r and is equally likely to occur for any infective, regardless of the degree. Therefore, the distribution for the degree minima is the same as the degree distribution for infectives. Figure 10.10b shows good agreement between the observed distribution of minima and that expected from the infective degree distribution (which was found from Monte Carlo simulations in [29]).

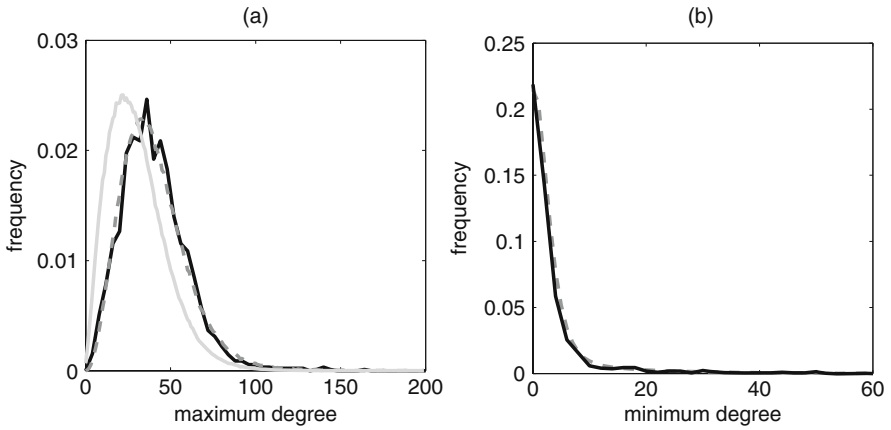

Fig. 10.10 Statistics for degree time series. *Black curves*: observed distributions; *dashed gray curves*: expected distributions. (**a**) Distribution of local maximum degrees. The degree distribution for susceptibles is shown in *light gray* for reference. (**b**) Distribution of local minimum degrees. Parameters: $p = 0.002$, $q = 0.0016$, $r = 0.002$, $w = 0.04$

Degree maxima occur immediately before a susceptible becomes infected. The infection rate depends on the number of infected neighbors a susceptible node has, which is almost directly proportional to its degree. (See [29] for details.) Letting d represent the degree of a susceptible and P_d the degree distribution for susceptibles, we thus expect the infection rate to be proportional to d and the distribution of degree maxima to be proportional to dP_d. This expected distribution is shown in Fig. 10.10a, and there is again good agreement with the observed distribution of maxima and the expected values. The degree distribution for susceptibles is shown for reference. The distribution of maxima is skewed to higher degrees because of the dependence of the infection process on node degree.

To develop a complete understanding of these processes, a theory to predict the degree distributions from first principles is needed. Such a theory must account for correlations between the infection status of an infective and its neighbors, as explained in [29].

10.8 Conclusions and Discussion

In this chapter, we considered a model of an adaptive network and its fluctuations. We introduced a model based on an SIRS epidemic structure which included transition probabilities between node states as well as link dynamics. In this model, the link dynamics are a function of the state variables, and since the state variables depend on the links, it forms a closed feedback system between nodes and links. The model is an extension of, and contains in the limit of large resusceptibility rate q, the SIS model studied in [19]. The fluctuations of the model were simulated in two ways: The full system was studied via Monte Carlo simulation on a finite population. In addition, a low dimensional approximation was studied using a Langevin simulation with an additive noise term to the mean field equations.

Quantifying where the system is most sensitive to fluctuations required an examination of the bifurcation structure of the deterministic mean field equations. For the steady states of the mean field equations, we examined the locations of both Hopf bifurcations and saddle-node points. We saw that as the resusceptibility rate q changes, the type of bifurcation changes. In general, for large q, we have a generic saddle-node bifurcation, while for small q we have a saddle-saddle bifurcation giving rise to a Hopf bifurcation.

Fluctuations were examined with respect to these bifurcations, and particular attention was paid to the large and small q cases. This led us to examine the specific role of the recovered class in the SIRS model as compared with the limiting case of the SIS model. In the SIS case, we found that without the recovery class, newly created susceptibles may be still connected to another infective, and thus may become reinfected immediately. This mechanism led to a reduction in the fluctuations of infectives. On the other hand, the inclusion of the recovery class introduced a mean delay time prior to potential reinfection, thereby increasing infective fluctuations.

By examining the fluctuation sizes near the bifurcation points, we found the existence of scaling laws in both the mean field model and the full system. Comparing

the stochastic dynamics of SIRS and SIS cases, we examined the effect of the rewiring rate w and resusceptibility rate q on the fluctuations. For a large range of q values, we showed the existence of a scaling law near the Hopf bifurcation, which includes the fluctuations for the limiting SIS case. We found that for small q values, the fluctuations change more rapidly with rewiring rate w than they do for the SIS model, making fluctuations more sensitive with respect to parameters in the SIRS case. Other effects, such as latency, or delay, between infective nodes and non-infected neighbors occur in the SIRS model but not the SIS model.

The degree fluctuations are still difficult to predict, although some of these phenomena can be understood in certain cases. However, much work still is required to understand the fluctuations of the network geometry. Current tools for the analysis of static networks are insufficient to make predictions about adaptive networks. A complete understanding of the dynamics, fluctuations, and geometry in the future requires tools which incorporate topology, stochastic dynamics, and time dependent graph theory.

Because adaptive networks based on epidemiology contain many of the features of adaptive networks in general, we expect them to continue to reveal new and interesting dynamic phenomena as they are extended for more detailed modeling of social situations, including and beyond those of infectious disease spread.

Acknowledgements This work was supported by the Office of Naval Research and the Armed Forces Medical Intelligence Center. LBS was supported by the Jeffress Memorial Trust.

References

1. R. M. Anderson and R. M. May. *Infectious Diseases of Humans.* Oxford University Press, Oxford, 1991.
2. L. Arnold. *Random Dynamical Systems*. Springer, New York, 2001.
3. A. Barabási and R. Albert. Emergence of scaling in random networks. *Science*, 286(5439):509–512, 1999.
4. I. J. Benczik, S. Z. Benczik, B. Schmittmann, and R. K. P. Zia. Lack of consensus in social systems. http://arxiv.org/abs/0709.4042, 2007.
5. S. Bornholdt and T. Röhl. Self-organized critical neural networks. *Physical Review E*, 67(6):066118, 2003.
6. S. Bornholdt and K. Sneppen. Neutral mutations and punctuated equilibrium in evolving genetic networks. *Physical Review Letters*, 81(1):236–239, 1998.
7. K. Christensen, R. Donangelo, B. Koiller, and K. Sneppen. Evolution of random networks. *Physical Review Letters*, 81(11):2380, 1998.
8. L. D. Costa, F. A. Rodrigues, G. Travieso, and P. R. V. Boas. Characterization of complex networks: A survey of measurements. *Advances in Physics*, 56:167–242, 2007.
9. E. J. Doedel, R. Paffenroth, A. Champnets, T. Fairgrieve, Y. A. Kuznetsov, B. Sandstede, and X. Wang. *AUTO: Software for continuation and bifurcation for ordinary differential equations*, 2001.
10. M. I. Dykman and M. A. Krivoglaz. Fluctuations in non-linear systems near bifurcations corresponding to the appearance of new stable states. *Physica A*, 104(3):480–494, 1980.
11. H. Ebel and S. Bornholdt. Coevolutionary games on networks. *Physical Review E*, 66(5): 056118, 2002.

12. G. C. M. A. Ehrhardt, M. Marsili, and F. V. Redondo. Phenomenological models of socioeconomic network dynamics. *Physical Review E*, 74(3):036106, 2006.
13. Z. Fan and G. Chen. Evolving networks driven by node dynamics. *International. Journal of Modern Physics B*, 18:2540–2546, 2004.
14. S. Gil and D. H. Zanette. Coevolution of agents and networks: Opinion spreading and community disconnection. *Physics Letters A*, 356(2):89–94, 2006.
15. P. M. Gleiser and D. H. Zanette. Synchronization and structure in an adaptive oscillator network. *European Physics Journal B*, 53:233–238, 2006.
16. P. Gong and C. van Leeuwen. Evolution to a small-world network with chaotic units. *Europhysical Letters*, 67:328–333, 2004.
17. R. Graham and T. Tél. Nonequilibrium potentials for local codimension-2 bifurcations of dissipative flows. *Physical Review A*, 35(3):1328–1349, 1987.
18. T. Gross and B. Blasius. Adaptive coevolutionary networks: a review. *Journal of the Royal Society Interface*, 2007. DOI: 10.1098/rsif.2007.1229.
19. T. Gross, C. J. D. D'Lima, and B. Blasius. Epidemic dynamics on an adaptive network. *Physical Review Letters*, 96:208701, 2006.
20. P. Holme and G. Ghoshal. Dynamics of networking agents competing for high centrality and low degree. *Physical Review Letters*, 96(9):098701, 2006.
21. P. Holme and M. E. J. Newman. Nonequilibrium phase transition in the coevolution of networks and opinions. *Physical Review E*, 74(5):056108, 2006.
22. W. Horsthemke and R. Lefever. *Noise-Induced Transitions: Theory and Applications in Physics, Chemistry, and Biology*. Springer Series in Synergetics , Vol. 15, 1983.
23. J. Ito and K. Kaneko. Spontaneous structure formation in a network of chaotic units with variable connection strengths. *Physical Review Letters*, 88(2):028701, 2002.
24. J. Ito and K. Kaneko. Spontaneous structure formation in a network of dynamic elements. *Physical Review E*, 67(4):046226, 2003.
25. S. Jain and S. Krishna. A model for the emergence of cooperation, interdependence, and structure in evolving networks. *Proceedings of the National Academy of Science*, 98: 543–547, 2001.
26. M. E. J. Newman. The structure and function of complex networks. *SIAM Review*, 45(2): 167–256, 2003.
27. J. M. Pacheco, A. Traulsen, and M. A. Nowak. Coevolution of strategy and structure in complex networks with dynamical linking. *Physical Review Letters*, 97:258103, 2006.
28. J. C. Scholz and M. O. W. Greiner. Topology control with ipd network creation games. *New Journal of Physics*, 8:185–199, 2007.
29. L. B. Shaw and I. B. Schwartz. Fluctuating epidemics on adaptive networks. *Physical Review E*, 77:066101, 2008.
30. B. Skyrms and R. Pemantle. A dynamic model of social network formation. *Proceedings of the National Academy of Sciences*, 97:9340–9346, 2000.
31. F. Vazquez, V. M. Eguíluz, and M. San Miguel. Generic absorbing transition in coevolution dynamics. *Physical Review Letters*, 100(10):108702, 2008.
32. D. H. Zanette and S. Gil. Opinion spreading and agent segregation on evolving networks. *Physica D*, 224:156–165, 2006.
33. D. H. Zanette and S. R. Gusman. Infection spreading in a population with evolving contacts. http://arxiv.org/abs/0711.0874, 2007.
34. C. Zhou and J. Kurths. Dynamical weights and enhanced synchronization in adaptive complex networks. *Physical Review Letters*, 96(16):164102, 2006.